Computer Methods and Programs in Biomedicine 210 (2021) 106380

Contents lists available at ScienceDirect

Computer Methods and Programs in Biomedicine

journal homepage: www.elsevier.com/locate/cmpb

Automatic landmark annotation in 3D surface scans of skulls: Methodological proposal and reliability study

Enrique Bermejo[a,d,*], Kei Taniguchi[a], Yoshinori Ogawa[a], Rubén Martos[b], Andrea Valsecchi[c,d], Pablo Mesejo[c,d], Oscar Ibáñez[c,d], Kazuhiko Imaizumi[a]

[a] Second Forensic Biology Section, National Research Institute of Police Science, Chiba 277–0882, Japan
[b] Physical Anthropology Lab, Dpt. of Legal Medicine, Toxicology and Physical Anthropology, University of Granada, Granada 18071, Spain
[c] Panacea Cooperative Research S. Coop., Ponferrada 24402, Spain
[d] Andalusian Research Institute in Data Science and Computational Intelligence (DaSCI), University of Granada, Granada 18071, Spain

ARTICLE INFO

Article history:
Received 24 March 2021
Accepted 22 August 2021

Keywords:
3D Automatic landmark annotation
Anatomical template alignment
Image registration
Craniofacial analysis
Computer-aided decision support systems

ABSTRACT

Background and Objectives: Craniometric landmarks are essential in many biomedical applications, such as morphometric analysis or forensic identification. The process of locating landmarks is usually a manual and slow task, highly influenced by fatigue, skills and the experience of the practitioner. Localization errors are propagated and magnified in subsequent steps, which can result in incorrect measurements or assumptions. Thereby, standardization, reliability and reproducibility lay the foundations for the necessary accuracy in subsequent measurements or anatomical analysis. In this paper, we present an automatic method to annotate 3D surface skull models taking into account anatomical and geometrical features.

Methods: The proposed method follows a hybrid structure where a deformable template is used to initialize the landmark positions. Then, a refinement stage is applied using prior anatomical knowledge to ensure a correct placement. Our proposal is validated over thirty 3D skull scans of male Caucasians, acquired by hand-held surface scanning, and a set of 58 craniometric landmarks. A statistical analysis was carried out to analyze the inter- and intra-observer variability of manual annotations and the automatic results, along with a visual assessment of the final results.

Results: Inter-observer errors show significant differences, which are reflected in the expert consensus used as reference. The average localization error was 2.19 ± 1.5 mm when comparing the automatic landmarks to the reference location. The subsequent visual analysis confirmed the reliability of the refinement method for most landmarks.

Conclusions: Repeated manual annotations show a high variability depending on both skills and expertise of the observer, and landmarks' location and characteristics. In contrast, the automatic method provides an accurate, robust and reproducible alternative to the tedious and error-prone task of manual landmarking.

1. Introduction

Studies involving any form of craniofacial analysis require the location of anatomical structures, usually relying on landmarks, or reference points, defined over bone (craniometric) or soft-tissue (capulometric) structures. Landmark-based analysis is an integral part of several tasks in medicine, dentistry, and forensic anthropology, such as craniofacial surgical planning [1], orthodontics [2,3], morphometrics [4], or human identification [5], among others.

Not all anatomical landmarks are equally identifiable. According to Bookstein [6], landmarks can be classified in three types or categories. Type I landmarks are located at the intersection of sutures or tissues. Landmarks defined at points of maximum curvature or local geometric information belong to Type II. Meanwhile, Type III refers to extremal landmarks, defined in terms of the location of other landmarks or the orientation of the object. Generally, Type I landmarks are considered to be anatomically homologous and easily identifiable with precision.

* Corresponding author.
E-mail addresses: enrique@nrips.go.jp, enrique.bermejo@decsai.ugr.es (E. Bermejo).

https://doi.org/10.1016/j.cmpb.2021.106380

The task of manual landmark localization is considered error-prone and time consuming, while it demands a high level of expertise. Reliability and reproducibility studies found that: i) a localization error is inherent to the task [7,8], ii) the magnitude of the error depends on the landmark category [9,10] (type I, II, or III), and iii) the use of different imaging systems (2D, 3D) or annotation software can introduce bias in the process [11–15].

To address the subjectivity of manual landmark annotation, numerous approaches have been proposed in the literature, aiming at automatizing the procedure. These techniques benefit from digitization advances in the field, such as the increasing availability of digital collections of 3D data for archival purposes [16], or the use of advanced imaging techniques to acquire high-resolution digital models of facial morphology and skeletal bone [17,18]. Automatic methods can be classified into three large groups: knowledge-based, template-based, and learning-based [19].

Knowledge-based approaches rely on geometric or anatomical characteristics retrieved using computer vision tools: image segmentation, feature extraction, edge and contour detection, among others [20–22]. Their performance is highly influenced by the quality of the images or the complexity of the 3D models. Template-based models have been employed to address such limitations. The use of templates or statistical shape models [23] has been widely considered to compare anatomical features, such as analyze the dimorphism of different individuals [24], reconstruct skeletal bone [25], or evaluate facial growth [26]. Commonly, a representative 2D image or 3D model is used as reference (template), and matched with the corresponding anatomical structure (target) or deformed to fit its shape [27–31]. Main drawbacks of template-based approaches are the complexity of the procedure and the necessity of parameter tuning to avoid inaccuracies when fitting the model.

In the last few years, learning-based methods have gained popularity due to recent advances in machine learning, neural networks and deep learning in particular. While approaches specifically oriented to 2D craniometric landmark localization obtained accurate results [32], their 3D counterparts encountered more difficulties due to the higher complexity of dealing with 3D imaging data [33]. Learning-based approaches require a great amount of training data to properly generalize and obtain competitive results [34,35]. Such requirement entails considerable disadvantages given the absence of large and public databases to train the models, and considering that the manual annotation process is time-consuming and unreliable.

Taking into account the existing limitations of current methods in the literature, the aim of this study is to introduce a novel approach to automatically annotate craniometric landmarks. Our proposal has been designed for applications where skeletal bone may not be well preserved or present fractures. Therefore, the main contribution of this paper is a hybrid (template- and knowledge-based) method to locate landmarks in 3D surface models of skulls. Such design was considered to maximize the accuracy of locating anatomical structures and to expedite the annotation procedure in order to assist the practitioner.

2. Materials and methods

The dataset used in this study consists of 3D models of twenty male adult skulls of Caucasian ancestry. It was collected at the University of Vilnius (Lithuania), by using a hand-held surface scanner, Go!SCAN 20^{TM}. The scanned human remains (skulls and mandibles) belong to the executed leaders of the January Uprising of 1863–1864, that were uncovered at the Upper Castle of Vilnius in 2017 [36]. Ten of these skulls are in good conditions, while the rest present problems such as incomplete denture, fragmented regions due to physical trauma, or scanning errors (low visual resolution, missing occluded areas), as shown in Fig. 1. The dataset was complemented with an additional set of ten modern skulls from male Caucasian adults dating back three decades. The corresponding 3D surface models were acquired in similar conditions at the University of Granada (Spain) and were considered to provide an overview of the performance of our proposal in different situations.

Fig. 1. Illustration of the missing dentition or fragmentation state of some models in the dataset.

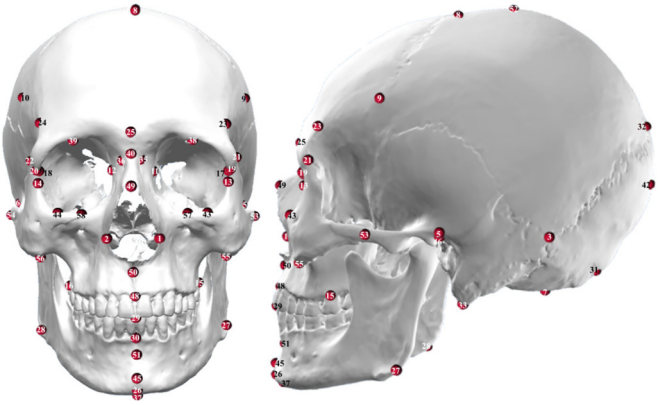

Fig. 2. Visualization of the landmark distribution across the whole skull anatomy.

A set of 38 standardized craniometric landmarks (18 unilateral and 20 bilateral, 58 in total) were annotated across the whole skull [37,38], as described in Table 1 and shown in Fig. 2. The list encompasses a subset of type I, II, and III landmarks [6], commonly used in anatomical studies. This landmark set was manually annotated by a group of three forensic anthropologists with different training and levels of expertise. Participants were instructed to space annotations in time during one month to avoid bias, and only to locate those landmarks they could precisely place. Reported times for annotating a single skull were variable, within thirty minutes. Additionally, an intra-observer study on the dispersion of the manual landmarks was considered over a subset of the dataset. In this latter study, all the observers carried out three rounds of annotations in total, over five of the thirty skulls, one month after the initial analysis. Results of the intra-observer analysis are shown as supplementary material.

For each skull and landmark, we calculated the averaged location marked by the expert, which is meant to represent the consensus location of different observations. For clarity, we called this the experts average localizations (EAL). Often, this reference coordinates are used as ground-truth data to assess the results obtained by some landmarking method, or to either train or test a machine learning approach. However, one can identify two important drawbacks to this approach. First, when the task at hand is very subjective and the data is provided by a small number of observers, there is no guarantee that the EAL actually represent the best locations. Second, our objective is not to reproduce how trained professionals locate landmarks, but rather to locate land-

Table 1
Craniofacial landmark definition according to Caple and Stephan [37]. Frontomalare anterior follows the definition provided by Howells [38]. Last columns indicate the category of the landmark according to Bookstein [6], and the refinement technique applied. No refinement is applied to those marked with '-'.

Landmark			Definition	T	R
1/2	Alare	al	Most lateral point on the nasal aperture in a transverse plane determined by instrument	III	**c**
3/4	Asterion	ast	Point located on the intersection of the parietal, temporal, and occipital bones	I	-
5/6	Auriculare	au	On the zygomatic root, vertically above the center of the external auditory meatus	II	**l**
7	Basion	ba	Median plane at the anterior extent of the foramen magnum. It can be the most posterior aspect or the most inferior median point on the foramen magnum's anterior rim	II	**l s**
8	Bregma	b	Located where the sagittal and coronal sutures meet	I	**r**
9/10	Coronale	co	Most lateral point on the coronal suture	III	-
11/12	Dacryon	d	Point on the medial border of the orbit where the lacrimomaxillary suture meets the frontal bone	I	-
13/14	Ectoconchion	ec	Lateral point on the orbit at a line that bisects the orbit transversely	II	-
15/16	Ectomolare	ecm	Most lateral point on the lateral surface of the alveolar crest, along the second molar on the maxilla	III	**c**
17/18	Frontomalare anterior	fma	Most anterior projecting point on the frontomalare suture	III	-
19/20	Frontomalare orbitale	fmo	Point located on the orbital rim marked by the zygomaticofrontal suture	II	-
21/22	Frontomalare temporale	fmt	Most lateral part of the zygomaticofrontal suture	III	-
23/24	Frontotemporale	ft	Most anterior and medial point of the inferior temporal line, on the zygomatic process of the frontal bone	II	-
25	Glabella	g	Most projecting anterior median point on lower edge of the frontal bone, on the brow ridge, between the superciliary arches and above the nasal root	II	**l s**
26	Gnathion	gn	median point halfway between pogonion and menton	III	**i**
27/28	Gonion	go	Point on the rounded margin of the angle of the mandible, bisecting two lines one following vertical margin of ramus and one following horizontal margin of corpus of mandible	II	**l**
29	Incision	inc	Point at the occlusal surface where the upper central incisors meet	II	**l s**
30	Infradentale	id	Median point at the superior tip of the septum between the mandibular central incisors	II	**l s**
31	Inion	i	Median point between the apices of the superior nuchal lines at the base of the external occipital protuberance	II	**l s**
32	Lamda	l	Point at which the two legs of the lamboid suture and sagital suture meet	I	**r**
33/34	Mastoidale	ms	Most posterior point of the mastoid notch	II	**l**
35/36	Maxillofrontale	mf	Located at the intersection of the anterior lacrimal crest with the frontomaxillary suture	I	-
37	Menton	me	Most inferior median point of the mental symphysis	III	**l s**
38/39	Mid-supraorbital	mso	Point on the anterior aspect of the superior orbital rim, at the line that vertically bisects the orbit	II	**c**
40	Nasion	n	Located as the intersection of the naso-frontal sutures in the median plane	I	**l s**
41	Ophistion	o	Median point on the anterior side of the foramen magnum's posterior rim	II	**l s**
42	Opisthocranion	op	Most posterior median point of the occipital bone, instrumentally determined as the greatest chord length from glabella	III	**i**
43/44	Orbitale	or	Most inferior point on the inferior orbital rim. Usually falls along the lateral half of the orbital margin	II	**c**
45	Pogonion	pg	Most anterior median point on the mental eminence of the mandible	III	**l s**
46/47	Porion	po	Most superior point on the upper margin of the external auditory meatus	II	-
48	Prosthion	pr	Median point between the central incisors on the anterior margin of the maxillary alveolar rim	II	**l s**
49	Rhinion	rhi	Most rostral (end) point on the internasal suture	I	**l**
50	Subspinale	ss	Deepest point seen in the profile view below the anterior nasal spine (point A)	II	**l**
51	Supramentale	sm	Deepest median point in the groove superior to the mental eminence (point B)	II	**l s**
52	Vertex	v	Most superior point of the skull with respect to the mid sagittal plane	III	**l s**
53/54	Zygion	zy	Most lateral point on the zygomatic arch	III	**l**
55/56	Zygomaxillare	zm	Most prominent point located at around the lower end of the zygomaxillary suture	III	-
57/58	Zygoorbitale	zo	Point of intersection between zygomaxillary suture and orbit border	II	**l**

marks according to their definition. Such definitions often imply calculations or the evaluation of geometric properties, such as being the median point between two other landmarks, or the most later point in an area. It is not hard to imagine that an automatic method could locate a median point with higher precision than a group of observers. However, if we were to evaluate the algorithm only by comparing its output against the EAL, there would be no way for the algorithm to actually outperform the human observers.

To address these issues, we performed a subsequent validation study where human observers were asked to evaluate both EAL and the automatic localizations in terms of compliance with the landmarks definition. Three observers participated in a blind experiment to ascertain the most precisely located landmarks over the same five skulls considered in the intra-observer study. Two of the three observers were not involved in the previous annotation procedure. During the validation, the practitioners performed a visual assessment of both localizations using the open-source software Meshlab (meshlab.net). No reference was provided on which coordinate belongs to the expert consensus or the automatic method.

3. Technical procedure

3.1. Manual annotation

Manual landmarks were recorded using the software Skeleton-ID™ (skeleton-id.com), which allows practitioners to visualize the 3D models and locate points guided by a toolset (see Fig. 3) de-

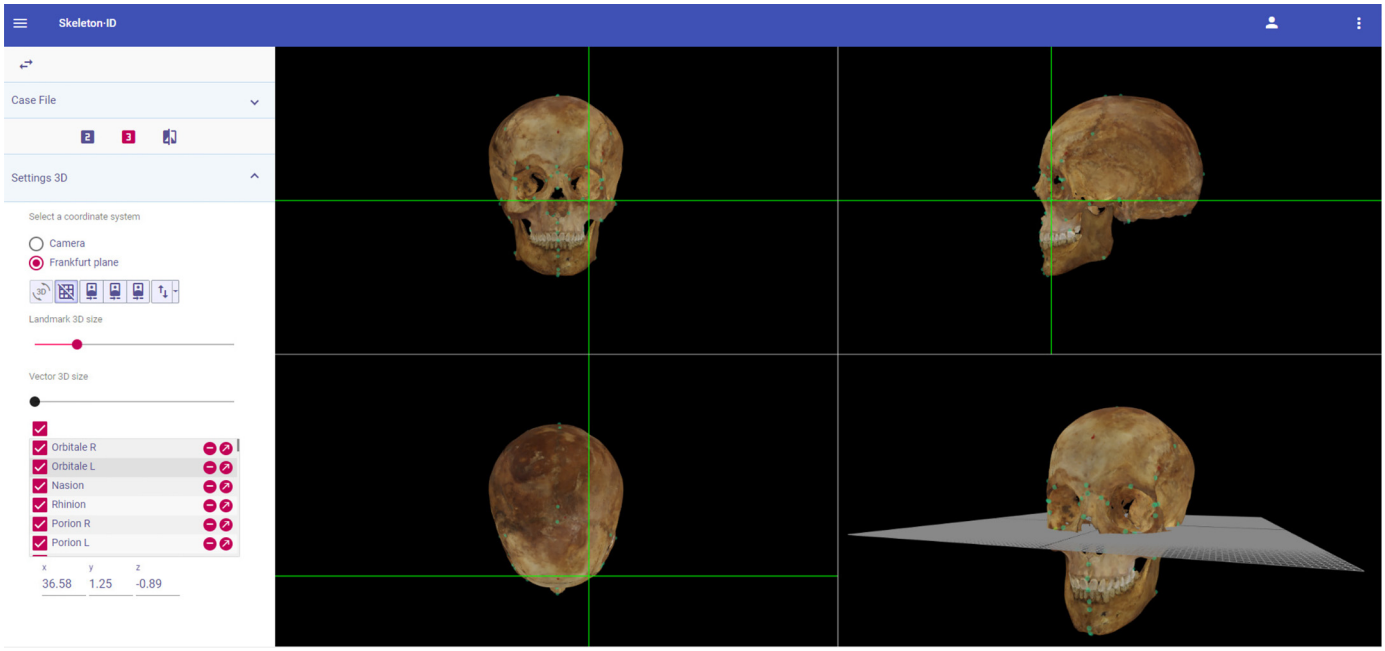

Fig. 3. Anatomical planes available in Skeleton-ID to assist with the landmark annotation process.

signed to improve the precision of the procedure (as recommended by MEPROCS [39]). The online service includes tools to:

- Set the 3D model in the Frankfort Horizontal plane [40], following the convention of 1884 to orient objects in anatomical standard position.
- View the cranial norms in 4 simultaneous windows, three of them displayed according to the Frankfort Horizontal plane, easing the location and refinement of craniometric points.
- Crosshair and traverse auxiliary 3D lines to increase the precision of locating craniometric points related to other points or anatomical structures. This tool allows the user to interact with two views at the same time, unequivocally locating the most anterior or posterior point in a region within the surface of the 3D model.

3.2. Automatic landmark initialization

The Meshmonk registration framework[1] [41] is used to automatically provide an initial set of landmarks for a target skull. The procedure follows a template-based strategy where a reference 3D mesh is aligned and elastically deformed to generate a homologous model of the target mesh (non-rigid registration). A homologous surface establishes a correspondence between the vertices of the template and the target surface. Thus, landmarks placed on the template can be located on the same vertex point of the homologous model and then projected (mapped) onto the anatomically equivalent point of the target surface. As the vertex index of the template landmark is known, the corresponding 3D coordinate after the elastic deformation will also be known. Then, the new location in the 3D space for each landmark is directly mapped onto the nearest vertex of the target surface. Fig. 4 summarizes this automatic annotation procedure, where the first step involves building an annotated template model as part of the design of the proposed method. The template generation is a semi-automatic step required only once before the proposed method can be applied automatically.

[1] Open-source implementation available at: https://github.com/TheWebMonks/meshmonk

The reference template is created following an iterative procedure, as described in [42]. Here, ten of the target skulls in better conditions were used to avoid bias due to missing surface information. Initially, all the mesh surfaces are realigned into a common coordinate system using generalized Procrustes analysis (GPA), along with the manual annotations. A random skull model from the database can be used to provide a reference framework for building an annotated template with a fixed number of vertices and faces (Fig. 4.a). This model was manually edited to repair surface errors and decimated to a final number of 154,328 vertices using Meshlab. For each mesh in the subset, the initial template is deformed into a corresponding homologous surface. Then, these models are averaged into a new template mesh, which is used for the next iteration. The process is repeated three times until convergence, which results in a smoothed 3D skull with no individualizing characteristics. Template landmarks are initialized as the average of the aligned EAL coordinates, located onto the template mesh vertices.

Once the generation stage is completed, the system is ready to automatically transfer landmarks into any target skull by applying the template mapping procedure (Fig. 4.b). The computational time required by the initialization step is variable, as it depends on the resolution of the 3D meshes (number of vertices), and the deformable registration iterations. For the 3D models considered in this work and 200 iterations as recommended in [41], the processing time ranges between three and ten minutes per skull model.

3.3. Anatomical refinement

After the initialization, a refinement stage is applied. Our proposal incorporates the anatomical information from the landmark standard definitions into a knowledge-based refinement procedure. The procedure is then guided by a series of geometric cues to improve the precision of the automatic landmarks placement within a small region of interest. The radius of this regions has been empirically determined as the Euclidean distance error between the mapped landmarks and the EAL as follows. For the three iterations of the template generation procedure (Fig. 4.a), the resulting errors of the mapped landmarks were logged before computing the

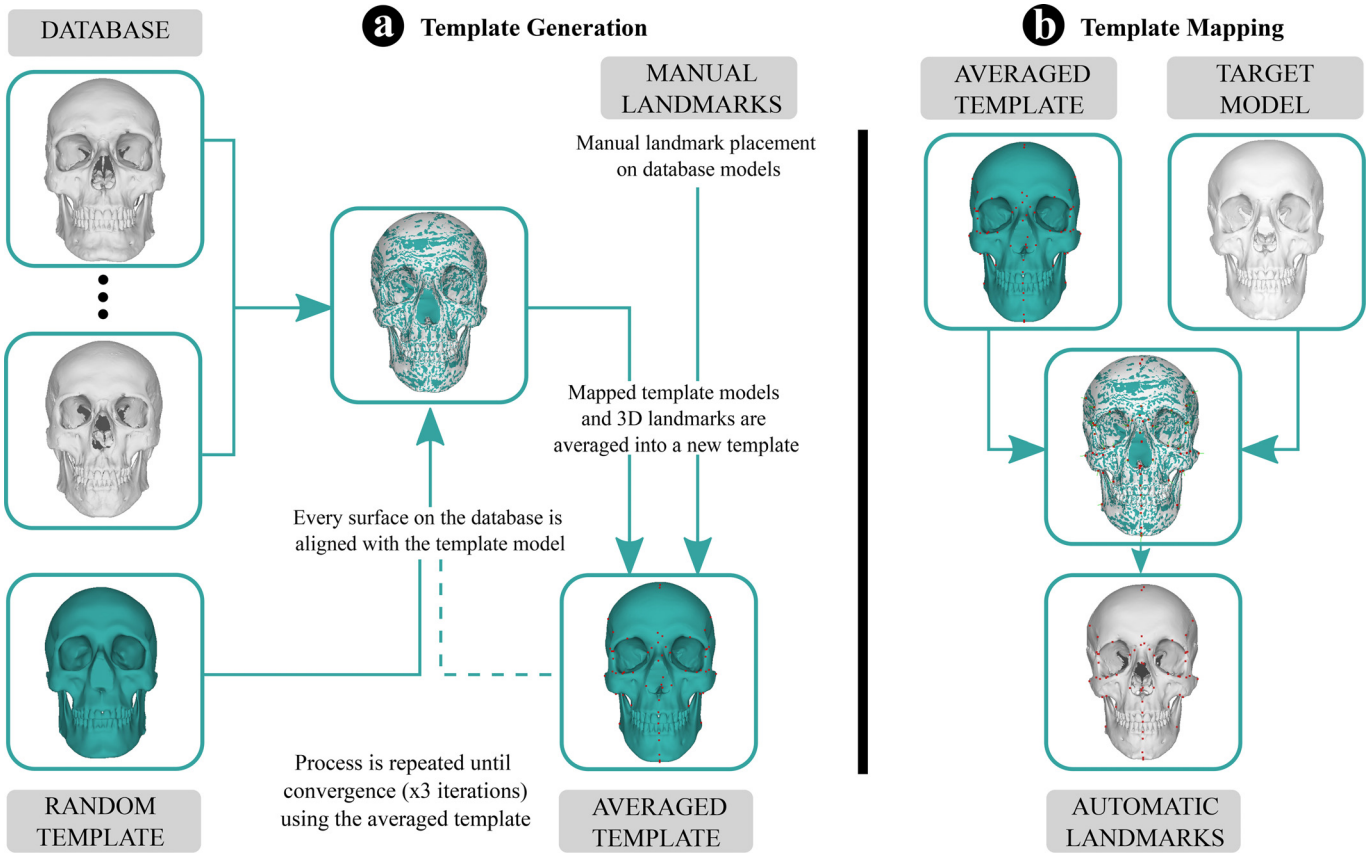

Fig. 4. Workflow of the automatic landmark initialization using the Meshmonk framework. (a) Template generation by averaging 3D models and landmark coordinates. (b) Template mapping and landmark transfer to a target model.

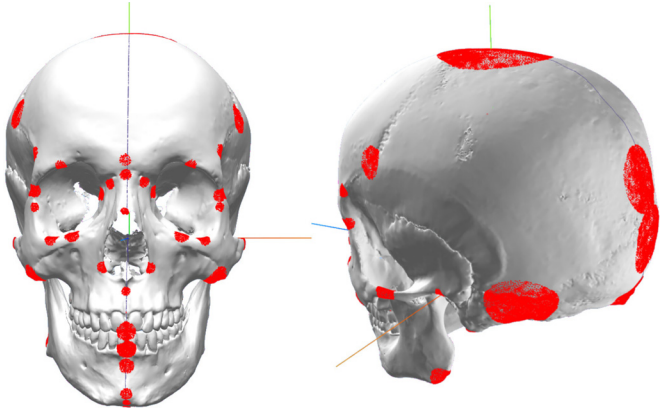

Fig. 5. Illustration of the neighborhood areas (in red) where the refinement technique is applied. (For interpretation of the references to colour in this figure legend, the reader is referred to the web version of this article.)

averaged template. Then, for each landmark, the radius was set according to the 75th percentile of the logged error distribution according to the ten considered skulls. Fig. 5 depicts (red) the radius of the search areas around each landmark.

In particular, we have developed a set of custom-designed heuristics or refinement approaches on how to displace the initial landmark coordinates (see Fig. 6). Our approach is versatile, as multiple heuristics can be combined depending on the landmark definition. The refinement approaches considered in our proposal are:

- *Symmetry (s).* Landmarks defined along the median or mid-sagittal plane, which vertically divides the skull in two sections, are displaced onto the closest mesh vertex that fits the symmetric plane of the skull (Fig. 6a). Following the approach described in [43], the reflectional symmetry of a skull model is automatically extracted. Then, the contour points of the intersection between the skull model and the symmetry plane are used to refine the location of the landmarks.
- *Contour information (c).* A set of 2D projections of different areas of the 3D skull model are extracted in order to find points along the contour of the orbital and nasal cavities. Contour points provide auxiliary information such as vertical and horizontal bisections to support the refinement (Fig. 6b). Initialized landmarks provide sufficient information to define a 3D bounding box around the areas of interest from which a section of the mesh is extracted. A perspective camera model, positioned at the minimum distance that encompasses the mesh section in the scene and oriented towards the center of the bounding box, is used to simulate the 2D projection.
- *Local curvature (l).* Within a reduced neighborhood area around a candidate landmark, the 3D mesh is locally explored according its geometric information. Knowledge of the mesh orientation and the 3D vertex coordinates allow us to search for extremal points inside a neighborhood according the coordinate planes. A subset of geometric heuristics is thus defined to extract the most *superior/inferior, anterior/posterior*, or *lateral left/right* neighbor vertex in the surface of the mesh to refine the landmark placement (Fig. 6c).
- *Ridges (r).* Cranial sutures provide a clear reference on where to locate anatomical landmarks. However, suture detection is not a trivial task, as it depends on the quality of the 3D model. Assuming the lack of high-resolution models and texture, we restrict its application to two landmarks placed in the most visible sutures: bregma and lamda. A 2D projection of the skull is

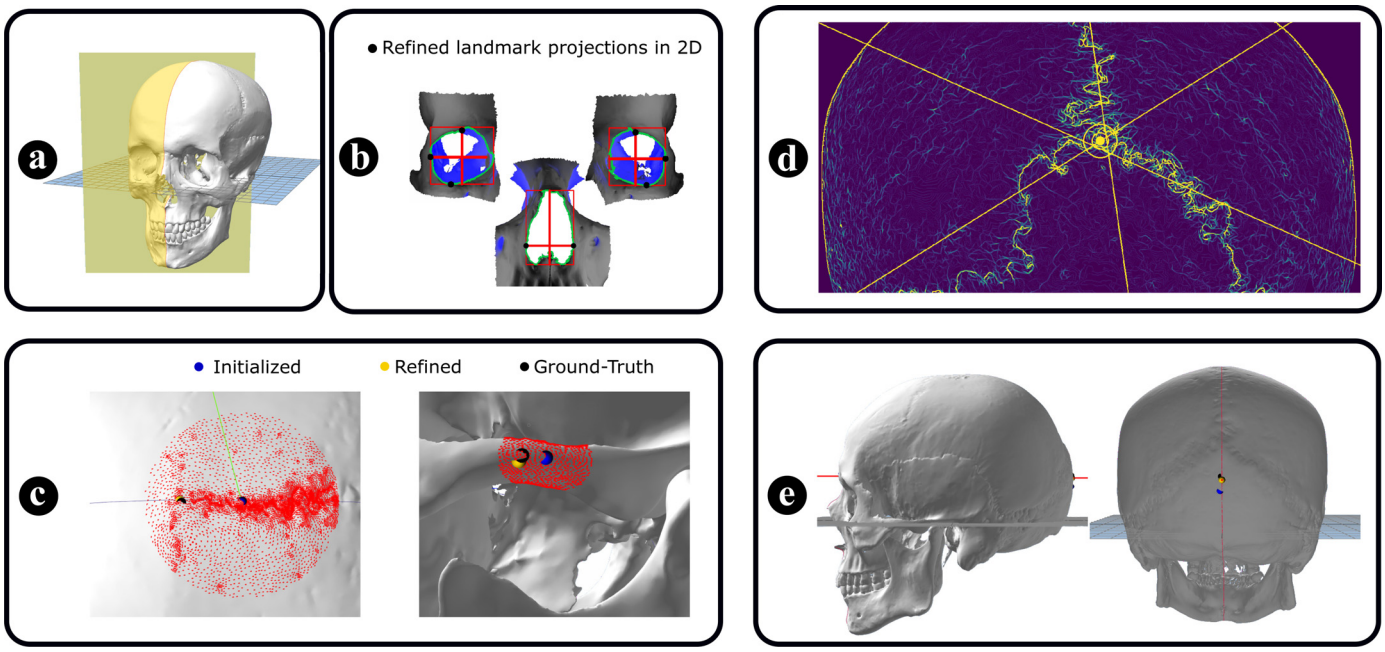

Fig. 6. Visualization of the different approaches for landmark refinement: (a) mid-plane detection; (b) contour and bisect lines detection; (c) local curvature analysis to displace vertex (left), and zygion L (right); (d) Ridge detection to locate lamda; (e) Automatic measurement of greatest chord length to displace opisthocranion.

extracted by positioning a virtual camera oriented towards the initialized landmark, which provides an overview of the skull surface around the region of interest. Then, the 2D projection is analyzed to find salient features corresponding to the cranium sutures by using the ridge detection filter implemented in OpenCV [44]. With this approach, the edges of the cranial sutures are easily detected as individual feature points on the image. A line corresponding to each visible suture is fitted on the detected points using the least squares method to provide reference of the suture trajectories. Finally, the intersection point between the trajectories of cranial sutures is estimated (Fig. 6d). The application of this heuristic is conditioned to the visibility of cranial sutures.

- *Instrumental (i).* For those landmarks whose definition is instrumentally related to others (i.e., median point between two landmarks), we defined a specific rule. The geometric calculation is performed once the related landmarks are refined to ensure a correct placement (Fig. 6e). Then the average point in the euclidean space between landmarks is computed and displaced onto the closest vertex of the target mesh.

The proposed heuristics share a common procedure whenever the mesh surface is analyzed to search for the closest vertex of a 3D coordinate or an extremal point within a neighborhood (*local curvature*). In the first place, the mesh vertices are indexed inside a binary search tree, known as K-D Tree [45]. Then, the search for the refined point within the region of interest (radius distance) is carried out by looking at the neighborhood of vertices around each mapped landmark. This method is called k-nearest neighbors algorithm (k-NN). Vertex indexation allows for a rapid access to the mesh geometry, resulting in a refinement step where the multiple heuristics detailed above are processed in less than 20 seconds.

3.4. Summary of the pipeline

In order to provide an overview for the application of our hybrid proposal, we detail here the steps followed to automatize the task of landmark annotation, along the implementation details of the different modules involved.

Table 2
Summary of the mean (μ), standard deviation (σ), and median (M) Euclidean distance (mm) with respect to the EAL. Results are organized by landmark type and method.

	Manual		Initialization		Refinement	
Type	μ (σ)	**M**	μ (σ)	**M**	μ (σ)	**M**
I	1.5 (1.9)	0.8	3.1 (3.5)	2.0	3.1 (3.5)	2.0
II	1.5 (1.4)	1.1	1.8 (1.7)	1.3	1.7 (1.5)	1.3
III	2.0 (2.3)	1.2	2.7 (3.5)	1.6	2.2 (1.9)	1.6
Total	1.7 (1.3)	1.3	2.4 (1.7)	2.0	2.2 (1.5)	1.8

- *Template mapping:* The fist step involves the elastic deformation of the annotated template and the landmark mapping from the deformed template to the target model. The Meshmonk registration framework is used for this purpose [41].
- *Symmetry detection:* In parallel, the symmetric plane of the target skull is obtained using the method[2] proposed in [43].
- *Contour and ridge detection:* Once the landmarks are initialized onto the target mesh, their coordinate information is used to obtain 2D projections of the areas of interest in order to extract the relevant features used by the proposed heuristics. The computer graphics libraries Three.js[3] and Opencv [44] were used for this purpose.
- *Anatomical refinement:* The adhoc heuristics gather all the previous information and refine the location of the initialized landmarks using the K-D Tree implementation of Three.js for a fast neighborhood search.

4. Results

The resulting landmark coordinates from manual observations, the template fitting method, and our refinement proposal were compared in terms of the Euclidean distance error. The comparison was made considering the EAL of the manual observations as reference locations. Table 2 summarizes the total error between the manual observations, the template-based approach only, and

[2] Open-source implementation available at: https://github.com/aecins/symseg
[3] Open-source graphics library available at https://threejs.org/

Table 3
Mean error (μ) and standard deviation (σ) in *mm* reported for the proposed automatic landmarks after refinement. The percentage rate of landmarks below a 2 mm, 3 mm, and 4 mm threshold is also shown (%).

Landmark	μ (σ)	<2mm	<3mm	<4mm
al L	1.4 (0.8)	83	93	100
al R	1.6 (1.0)	80	90	97
ast L	6.4 (4.9)	11	25	43
ast R	5.7 (6.2)	11	21	43
au L	1.4 (0.7)	83	97	100
au R	1.4 (1.1)	80	90	97
ba	1.4 (0.7)	82	96	100
b	5.0 (3.4)	17	40	50
co L	3.8 (2.8)	20	60	77
co R	3.7 (2.4)	23	50	67
d L	2.2 (1.2)	60	73	90
d R	1.7 (1.0)	70	87	97
ec L	1.3 (0.7)	73	97	100
ec R	1.5 (1.2)	67	97	97
ecm L	3.4 (2.5)	44	59	63
ecm R	2.5 (2.4)	56	70	81
fma L	1.3 (1.0)	70	93	100
fma R	1.3 (1.0)	83	87	100
fmo L	1.5 (0.9)	67	93	100
fmo R	1.3 (0.9)	80	97	100
fmt L	1.8 (0.9)	70	87	100
fmt R	1.4 (0.9)	80	93	100
ft L	1.9 (1.2)	63	83	93
ft R	2.2 (1.2)	47	83	90
g	1.4 (0.7)	87	97	100
gn	1.2 (0.6)	90	100	100
go L	2.1 (1.2)	50	77	93
go R	2.5 (1.0)	30	53	97
inc	1.3 (1.4)	86	95	95
id	1.5 (1.8)	86	86	93
i	5.1 (3.8)	14	45	52
l	4.9 (3.3)	21	32	46
ms L	1.1 (0.7)	80	100	100
ms R	1.2 (0.6)	87	100	100
mf L	1.6 (0.7)	72	93	100
mf R	1.7 (0.9)	67	90	100
me	1.1 (0.6)	87	100	100
mso L	2.1 (1.3)	53	80	93
mso R	1.4 (0.8)	70	97	100
n	1.2 (0.8)	90	97	100
o	1.4 (0.9)	76	97	100
op	4.0 (2.7)	23	43	60
or L	1.9 (1.1)	53	90	97
or R	2.3 (1.3)	53	77	87
pg	1.3 (0.8)	73	100	100
po L	1.6 (1.0)	73	93	97
po R	2.0 (1.1)	47	87	97
pr	1.9 (2.3)	78	85	85
rhi	1.5 (0.9)	71	93	100
ss	1.0 (0.6)	90	100	100
sm	2.1 (1.4)	60	77	93
v	3.5 (2.2)	27	47	70
zy L	2.4 (1.6)	48	72	83
zy R	2.4 (1.4)	43	73	87
zm L	2.2 (1.3)	53	80	87
zm R	2.7 (2.8)	57	63	87
zo L	1.8 (1.3)	61	82	96
zo R	2.3 (1.5)	59	72	83

our proposed approach (that combines the refinement with the template-based initialization). A detailed comparison of the results for the proposed refinement method is shown in Table 3. Fig. 7 shows the localization error between manual observations, the automatic landmark initialization, and the refined landmarks. Additionally, Table S4 of the supplementary material includes a comparative study on the suitability of the template generation procedure (see Fig. 4.a) when the method is applied to anatomically different populations. The study analyzes differences in the results between two skull samples dated more than one century apart.

Table 4
Summary of the three pairwise Dunn tests performed. Manual annotations by the observers are noted as A, B, and C. Auto corresponds to the proposed refinement approach.

By Method	Z	p		By Type	Z	p
A - B	-4,67	$<\mathbf{10^{-6}}$	**Manual**	**I - II**	-4,79	$<\mathbf{10^{-6}}$
A - C	-6,19	$<\mathbf{10^{-9}}$		**I - III**	-8,64	$<\mathbf{10^{-17}}$
B - C	-1,42	0,01		**II - III**	-5,56	$<\mathbf{10^{-8}}$
A - Auto	-15,16	$<\mathbf{10^{-45}}$	**Auto**	**I - II**	3,07	$<\mathbf{0,05}$
B - Auto	-10,80	$<\mathbf{10^{-26}}$		**I - III**	-3,20	$<\mathbf{0,05}$
C - Auto	-9,59	$<\mathbf{10^{-21}}$		**II - III**	-8,15	$<\mathbf{10^{-15}}$

In summary, the analysis showed no substantial differences that could be attributed to bias in the template landmarks.

4.1. Statistical analysis

To analyze the performance of the proposed automatic method and the influence of the landmark category in the localization error, we performed a series of pairwise comparisons using the non-parametric Dunn's test [46]. The aim was to test the null hypothesis stating there is no difference between the compared groups for a considered level of significance $\alpha = 0.05$. The results of the statistical tests are summarized in Table 4. All statistics and analysis conducted in this work were performed in R, version 3.6.3 for Linux [47].

In particular, we performed three different comparisons: i) *by method*; studying the differences between the three manual observations and the automatic annotation, ii) *by type - manual*; analyzing the influence of the landmark category on the manual observations, and iii) *by type - auto*; comparing this influence on the automatic landmarks. The first analysis (*by method*) was considered to provide insight into the subjectivity of the manual annotations and the suitability of EAL as a measure of reference. The results of the statistical tests showed significant differences that can be attributed to both the method considered (manual observations vs. automatic) and the category of the landmarks. Nevertheless, differences are larger for the automatic method and Type III landmarks.

4.2. Validation analysis

The validation assessment was performed over the 36 landmarks where the refinement heuristics were applied (see Table 1). To verify the suitability of the resulting landmarks, three forensic experts quantified the number of cases where either the expert consensus or the refined coordinates were properly located according the anatomical landmark definitions. They also quantified the number of cases where the automatic location was considered equal or better than the reference location. In addition, a binomial test was performed for each landmark considering the following null hypothesis: *'There are no differences in quality between the location of the expert consensus (EAL) and the automatic landmark'*.

Table 5 summarizes the results of the validation study. The percentage of cases where the automatic refinement method achieved similar or better results than the expert consensus is 82%. The statistical tests strongly support the findings of the validation study. Results showed significant differences for 16 landmarks where the accuracy of the automatic method is remarkable.

5. Discussion

The motivation behind using a database of 3D scanned models is to portray a straightforward view of the applicability of our proposal to actual forensic identification scenarios. High-resolution medical images are not always available in many situations where

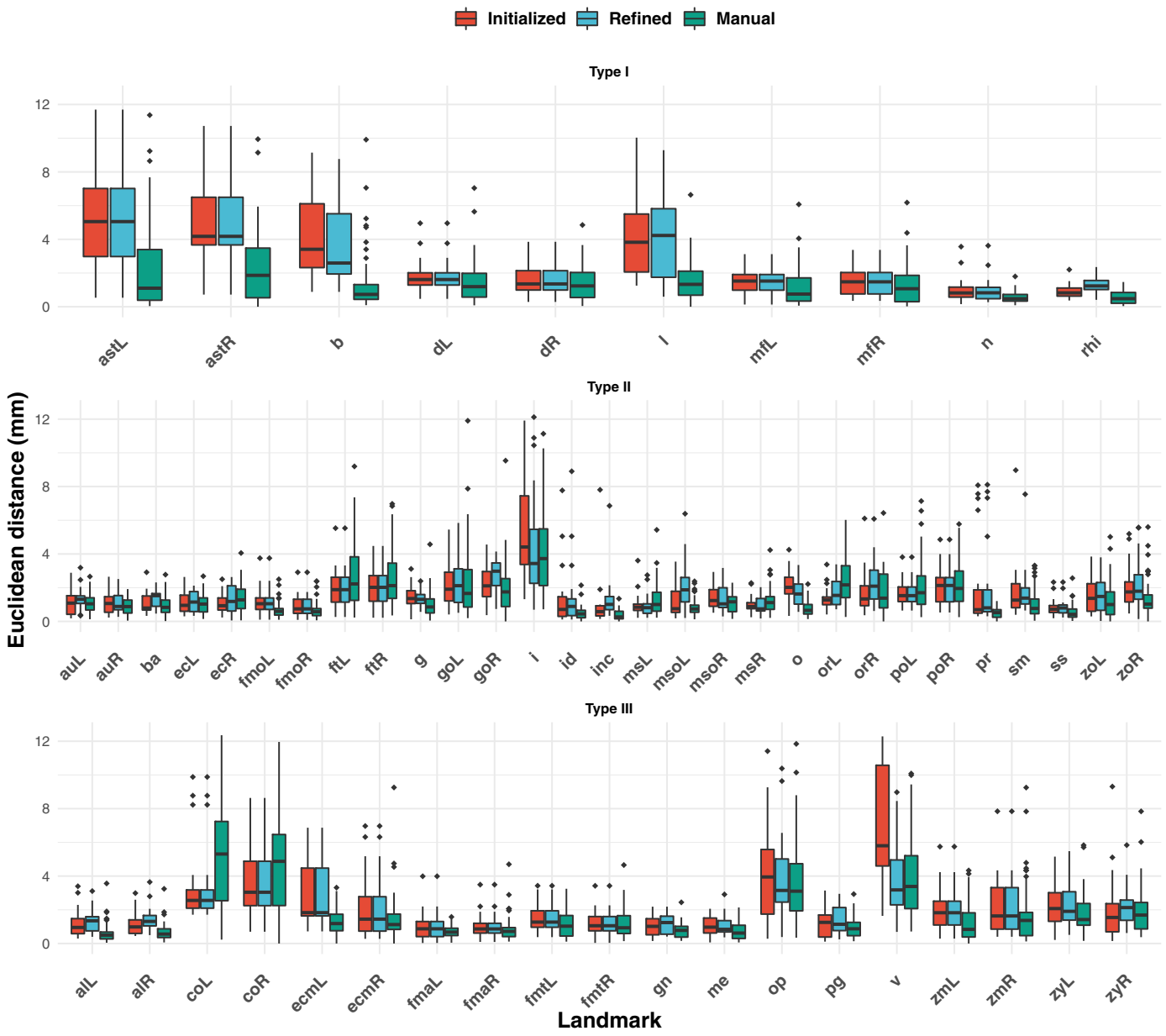

Fig. 7. Localization error box-plot for the manual observations, the template fitting, and the proposed refinement. Landmarks are organized by category. Outliers above 12 mm were not displayed in this graphic.

landmark analysis is required, and data can be either incomplete (i.e., fragmented skulls, partial denture, or missing landmarks) or unprocessed (3D models may present noise or holes in the mesh structure). During the initialization stage, the template-based deformation is able to provide a good fitting of the homologous models to the target skull models, regardless of its conditions. Thus, this stage allows for a method robust to fragmentation, holes in the 3D model or missing structures. We expect the use case of low quality or fragmented models to introduce additional sources of uncertainty in the procedure, especially during the homologous model fitting. However, the proposed method could be applied to different biomedical applications involving landmark annotation on 3D meshes. The only requirement would be using a 3D template adapted from a similar image modality, i.e., 3D models reconstructed from computed tomography (CT) data.

This study first analyzes the inter- and intra-observer dispersion. Results show that manual localization errors are consistent with studies in the literature (mean 1.62 ± 1.2 mm) [8,14]. As expected, each landmark presents a different degree of reliability. Repeated annotations by the same observer can also present a high variability, as shown in Tables S1 to S3 of the supplementary material. Statistical results for the inter-observer dispersion (upper left of Table 4) also found significant differences. While many elements influence the dispersion shown between observers, two main factors can provide an explanation: i) the difficulty of locating indistinct sutures (i.e., asterion or bregma) due to low image quality [48], and ii) the influence of distinct training or skills, which is noticeable for observer C (see Fig. S1 of the supplementary material) [49]. Regarding the influence of the landmark category on the localization error, manual observations present significant differences among the three types (I, II, or III). This conclusion is also consistent with other studies [50], and can be extrapolated to the automatic method.

The template fitting method provides a complete initialization of the landmark coordinates. Results show an average error for the 58 landmarks of 2.25 ± 1.6 mm, which is acceptable. However, this approach is sensitive to the quality of the 3D model and the variability of the manual annotations when building the template.

Table 5
Results for the validation analysis. First two columns show the percentage of cases where the expert consensus (EAL) and the refined landmarks (Auto) are properly located (%). Third column shows the percentage of cases where the refined landmark is considered to be equivalent or better than the expert consensus (Auto ≥ EAL). Last two columns show the results of the binomial tests, considering the raw p-value, and its adjustment for multiple comparisons. Values in bold are statistically significant for a confidence level of 95%.

	Accuracy			Binomial	
Landmark	**EAL**	**Auto**	**Auto ≥ EAL**	**p**	**adj-p**
al L	87	87	80	**0.04**	0.4
al R	87	80	80	**0.04**	0.4
au L	100	73	73	0.12	0.9
au R	87	87	87	**0.01**	0.1
ba	93	80	80	**0.04**	0.4
b	73	27	13	**0.01**	0.1
ec L	93	93	87	**0.01**	0.1
ec R	93	93	93	$<$**10^{-04}**	**0.03**
g	93	93	93	$<$**10^{-04}**	**0.03**
gn	93	100	100	$<$**10^{-05}**	**0.002**
go L	47	100	100	$<$**10^{-05}**	**0.002**
go R	73	100	93	$<$**10^{-04}**	**0.03**
inc	100	42	33	0.39	1.0
id	100	100	93	$<$**10^{-04}**	**0.03**
i	67	67	67	0.30	1.0
l	73	33	33	0.30	1.0
ms L	87	100	100	$<$**10^{-05}**	**0.002**
ms R	87	100	100	$<$**10^{-05}**	**0.002**
me	93	100	93	$<$**10^{-04}**	**0.03**
mso L	100	87	87	**0.01**	0.1
mso R	93	100	93	$<$**10^{-04}**	**0.03**
n	100	100	100	$<$**10^{-05}**	**0.002**
o	87	87	87	**0.01**	0.1
op	60	100	93	$<$**10^{-04}**	**0.03**
or L	73	93	87	**0.01**	0.1
or R	67	87	87	**0.01**	0.1
pg	100	100	93	$<$**10^{-04}**	**0.03**
pr	93	100	93	$<$**10^{-04}**	**0.03**
rhi	92	83	67	0.39	1.0
ss	100	100	100	$<$**10^{-05}**	**0.002**
sm	80	80	67	0.30	1.0
v	80	93	93	$<$**10^{-04}**	**0.03**
zy L	93	87	80	**0.04**	0.4
zy R	100	67	60	0.61	1.0
zo L	87	87	80	**0.04**	0.4
zo R	67	93	87	**0.01**	0.1

The statistical analysis shown in Table 4 (*by method*) indicates the dispersion found in manual observations is transferred to the automatic method through the expert consensus. In a recent study, Ridel et al. [31] measured the dispersion of using different template annotations on 1.64 mm, over 41 craniometric landmarks annotated on 10 skulls. Moreover, vertices among low curvature areas of the skull template present a higher variability in their location after the deformable registration. This issue mostly affects landmarks located in areas from the back of the skull and, especially, those placed at the intersection of sutures and bones (i.e., asterion, bregma, inion, lamda, or vertex). Landmarks in the dental area also show a slightly higher variability, which can be explained by the quality of the 3D mesh or the absence of teeth in some of the cases. This limitation justifies the application of the refinement stage proposed in this work.

After the refinement step, our proposal achieves an average error of 2.11 ± 1.5 mm for the 58 considered landmarks, slightly lowering the resulting deviation. On average, 64% of the landmarks are identified under a threshold error of 2 mm, 82% under 3 mm, and 89% under 4 mm. While the improvement in terms of error magnitude is not significant, the posterior refinement ensures the anatomical position of the coordinate is correct. Thus, the refinement is essential to minimize those cases where the initialization has displaced the landmark position during the template deformation.

The reliability analysis helps us identify landmarks where the automatic method behaves poorly, such as asterion, inion, or lamda, with results under 60%. When excluding such landmarks from the analysis (asterion, bregma, and lamda), automatic localization error for Type I landmarks falls to 1.5 mm, closely related to the error shown by manual annotations. In contrast to the precision of frontal landmarks, the lack of curvature information from areas at the back of the skull impairs the application of an accurate refinement strategy. We suggest a manual verification of landmarks where convoluted patterns may occur, such as partial sutural fusion or wormian bones, to ensure its correct placement when image quality is low. For those cases in the database where the ridge detection could be applied, suture landmarks bregma and lamda were correctly identified with an average error of 2.7 mm. Such results suggest we are addressing a *worst-case* scenario and the use of CT data can provide better performance due to higher detail visibility.

Localization errors achieved by the refinement method are comparable to other methods in the literature, where reported average errors are between 1.88 and 2.51 mm [21,29,30], and median errors around 2 mm [28]. While these results are similar to our proposal, it is not possible to directly compare the methods. The specific landmark set studied in each proposal is a determinant factor on the final magnitude of the localization error.

Our analysis also concurs with findings of Gupta et al. [21]. It can be argued that the considered EAL is not a valid evaluation method. The expert consensus presents high variability for some of the most used landmarks, i.e., orbitale, gonion, or vertex, among others. In the absence of a ground-truth or objective reference location, EAL provides a way to numerically compare our proposal with human practitioners. However, a complementary analysis is required, as the consensus location might displace the landmark away from its true location according the definition. The visual inspection performed during the validation study supports the previous assumption. EAL locations are not completely reliable due to the inter-observer variability between annotations. On the other hand, a visual analysis confirms that most refined landmarks are placed in equivalent or more precise anatomical locations. Landmarks that are easily located by computer-based methods still present a high amount of error when compared to the EAL. For example, opisthocranion and vertex, which show error distances of $\approx$4 mm, are also considered as highly reliable ($>$ 90%) during the visual validation performed by experts.

Once the template has been generated following the step of Fig. 4.a, the proposed method provides a complete automation of the 3D landmarking process without manual intervention. The annotation time is variable and depends mainly on the template fitting method, where computation time and registration accuracy can be balanced. The automatic method is able to provide results (as much as 6 times) faster than human observers for every case in the dataset considered in this work. This factor alone is of great importance, as our proposal can substantially expedite the completion time of tasks requiring landmark annotation, especially when multiple cases or collections of data are involved.

We identify some limitations in our study. Primarily, the dataset consists only on male skulls. The template suitability analysis found a similar precision when using a template in a population sample from a different time period. It indicates the method is, to some extent, robust to changes in the skull anatomy and the presence of individualizing features. However, other anatomical differences between very distinct populations may impact the performance of our proposal. In future works, we will analyze the influence of ancestry, age or sex in the generation of template models. Another limitation is the refinement of sutures. Currently, the

quality of the considered 3D models is crucial on the application of some refinement techniques. Thus, the coordinates of 11 of the 38 landmarks are not altered after initialization (noted with '-' in Table 1). As an alternative, texture information can be used to detect suture intersections when the quality of the 3D model is not sufficient.

6. Conclusions

The aim of this work is to introduce a novel automatic method to annotate landmarks on 3D surface models of skulls. Specifically, our proposal integrates two different approaches: a method based on a template model combined with the expert knowledge extracted from the standardized definition of craniometric landmarks. In addition, we analyze the reliability of a comprehensive set of landmarks (58 in total) across the entire anatomy of the skull, depending on its location and category.

Our proposal proved to be an accurate alternative to manual landmark annotation, robust to the deterioration condition of skulls. We found a clear advantage in locating Type II and III landmarks, located at regions with high curvature and extremal points, which minimizes the dispersion of landmarks where human experts tend to err. The results in terms of error against the expert consensus make our proposal suitable to be applied in several tasks while allowing a fast, reliable, and repeatable analysis of craniometric landmarks. The results of the refinement method confirm the effectiveness of our proposed approach combining a machine learning method with adhoc techniques based on expert knowledge.

Moreover, the introduced design can be adapted to the application at hand. Different templates can be used when different image modalities (surface models or CT scans) are involved, or fitted to distinct population samples. New refinement techniques can easily be integrated to improve the localization of alternative landmarks. In addition, any craniometric landmark could be considered as long as any of the policies can be applied for its refinement. Such versatility can introduce substantial benefits, for instance, in forensic identification applications where landmark analysis heavily depends on occlusion and visibility of facial features from photographs used as comparison.

Funding

Dr. Bermejo's work has been supported by the Japan Society for the Promotion of Science (JSPS) as International Research Fellow (Standard Fellowship).

Dr. Mesejo's work is funded by the European Commission H2020-MSCA-IF-2016 through the Skeleton-ID Marie Curie Individual Fellowship [Ref: 746592].

Dr. Valsecchi's work is funded by the Spanish Ministry of Science and Innovation grant [Ref: PTQ-17-09306]

Drs. Ibáñez work is funded by Spanish Ministry of Science, Innovation and Universities-CDTI, Neotec program 2019 [Ref: EXP-00122609/SNEO-20191236].

Additionally, This work was supported by the Grant-in-Aid for JSPS Fellows [Ref: 19F19119], by the Spanish Ministry of Science, Innovation and Universities, and European Regional Development Funds (ERDF), under grant EXASOCO [Ref: PGC2018-101216-B-I00], and by the Regional Government of Andalusia under grant EXAISFI [Ref: P18-FR-4262]. Funding for open access publication was provided by the University of Granada: CBUA.

Declaration of Competing Interest

The authors declare that they have no known competing financial interests or personal relationships that could have appeared to influence the work reported in this paper.

Acknowledgements

The authors would like to thank Rosario Guerra, staff at the Physical Anthropology Laboratory of the University of Granada for her cooperation during the data collection. In addition, we would like to thank Dr. Jankauskas and the team at the Department of Anatomy, Histology and Anthropology (University of Vilna, Lithuania) for collecting and sharing the 3D skull models used in this study.

Supplementary material

Supplementary material associated with this article can be found, in the online version, at doi:10.1016/j.cmpb.2021.106380.

References

[1] J.C. Kolar, E.M. Salter, Surgical Planning, Craniofacial anthropometry: Practical measurements of the head and face for clinical, surgical and research use., Charles C. Thomas Publisher, 1997.
[2] W.B. Downs, Variations in facial relationships: their significance in treatment and prognosis, Am J Orthod 34 (10) (1948) 812–840, doi:10.1016/0002-9416(48)90015-3.
[3] N.K. Kim, C. Lee, S.H. Kang, J.W. Park, M.J. Kim, Y.I. Chang, A three-dimensional analysis of soft and hard tissue changes after a mandibular setback surgery, Comput Methods Programs Biomed 83 (3) (2006) 178–187, doi:10.1016/j.cmpb.2006.06.009.
[4] A.H. Ross, A.H. McKeown, L.W. Konigsberg, Allocation of crania to groups via the "new morphometry", J. Forensic Sci. 44 (3) (1999) 14513J, doi:10.1520/jfs14513j.
[5] S. Damas, O. Cordón, O. Ibáñez, Handbook on craniofacial superimposition: The MEPROCS project, Springer International Publishing, 2020, doi:10.1007/978-3-319-11137-7.
[6] F.L. Bookstein, Morphometric tools for landmark data: Geometry and biology, Cambridge University Press, 1991, doi:10.1017/cbo9780511573064.
[7] T. Smektała, M. Jędrzejewski, J. Szyndel, K. Sporniak-Tutak, R. Olszewski, Experimental and clinical assessment of three-dimensional cephalometry: a systematic review, Journal of Cranio-Maxillofacial Surgery 42 (8) (2014) 1795–1801, doi:10.1016/j.jcms.2014.06.017.
[8] A. Sam, K. Currie, H. Oh, C. Flores-Mir, M. Lagravére-Vich, Reliability of different three-dimensional cephalometric landmarks in cone-beam computed tomography: a systematic review, Angle Orthodontist 89 (2) (2019) 317–332, doi:10.2319/042018-302.1.
[9] A.H. Ross, S. Williams, Testing repeatability and error of coordinate landmark data acquired from crania, J. Forensic Sci. 53 (2008) 782–785, doi:10.1111/j.1556-4029.2008.00751.x.
[10] B.R. Campomanes-Álvarez, O. Ibáñez, F. Navarro, I. Alemán, O. Cordón, S. Damas, Dispersion assessment in the location of facial landmarks on photographs, Int. J. Legal Med. 129 (1) (2014) 227–236, doi:10.1007/s00414-014-1002-4.
[11] J.B. Ludlow, M. Gubler, L. Cevidanes, A. Mol, Precision of cephalometric landmark identification: cone-beam computed tomography vs conventional cephalometric views, American Journal of Orthodontics and Dentofacial Orthopedics 136 (3) (2009) 312.e1–312.e10, doi:10.1016/j.ajodo.2008.12.018.
[12] O.J. van Vlijmen, T. Maal, S.J. Bergé, E.M. Bronkhorst, C. Katsaros, A.M. Kuijpers-Jagtman, A comparison between 2D and 3D cephalometry on CBCT scans of human skulls, Int J Oral Maxillofac Surg 39 (2) (2010) 156–160, doi:10.1016/j.ijom.2009.11.017.
[13] S.B. Sholts, L. Flores, P.L. Walker, S.K.T.S. Wärmländer, Comparison of coordinate measurement precision of different landmark types on human crania using a 3D laser scanner and a 3D digitiser: implications for applications of digital morphometrics, International Journal of Osteoarchaeology 21 (5) (2011) 535–543, doi:10.1002/oa.1156.
[14] N. Zamora, J.M. Llamas, R. Cibrián, J.L. Gandia, V. Paredes, A study on the reproducibility of cephalometric landmarks when undertaking a three-dimensional (3D) cephalometric analysis, Med Oral Patol Oral Cir Bucal 17 (4) (2012) e678–e688, doi:10.4317/medoral.17721.
[15] M. Cummaudo, M. Guerzoni, L. Marasciuolo, D. Gibelli, A. Cigada, Z. Obertovà, M. Ratnayake, P. Poppa, P. Gabriel, S. Ritz-Timme, C. Cattaneo, Pitfalls at the root of facial assessment on photographs: a quantitative study of accuracy in positioning facial landmarks, Int. J. Legal Med. 127 (3) (2013) 699–706, doi:10.1007/s00414-013-0850-7.

[16] S. White, C. Hirst, S.E. Smith, The suitability of 3D data: 3D digitisation of human remains, Archaeologies 14 (2) (2018) 250–271, doi:10.1007/s11759-018-9347-9.
[17] L. Ma, T. Xu, J. Lin, Validation of a three-dimensional facial scanning system based on structured light techniques, Comput Methods Programs Biomed 94 (3) (2009) 290–298, doi:10.1016/j.cmpb.2009.01.010.
[18] D. Errickson, I. Grueso, S.J. Griffith, J.M. Setchell, T.J. Thompson, C.E. Thompson, R.L. Gowland, Towards a best practice for the use of active non-contact surface scanning to record human skeletal remains from archaeological contexts, International Journal of Osteoarchaeology 27 (4) (2017) 650–661, doi:10.1002/oa.2587.
[19] K. Hung, C. Montalvao, R. Tanaka, T. Kawai, M.M. Bornstein, The use and performance of artificial intelligence applications in dental and maxillofacial radiology: a systematic review, Dentomaxillofacial Radiology 49 (1) (2019), doi:10.1259/dmfr.20190107.
[20] J.K. Liu, Y.T. Chen, K.S. Cheng, Accuracy of computerized automatic identification of cephalometric landmarks, American Journal of Orthodontics and Dentofacial Orthopedics 118 (5) (2000) 535–540, doi:10.1067/mod.2000.110168.
[21] A. Gupta, O.P. Kharbanda, V. Sardana, R. Balachandran, H.K. Sardana, A knowledge-based algorithm for automatic detection of cephalometric landmarks on CBCT images, Int J Comput Assist Radiol Surg 10 (11) (2015) 1737–1752, doi:10.1007/s11548-015-1173-6.
[22] M. Ed-Dhahraouy, H. Riri, M. Ezzahmouly, A. El Moutaouakkil, F. Bourzgui, H. Aghoutan, S. Belaqziz, Automatic localization of supraorbital and infraorbital foramina region on CBCT images, in: Advances in Intelligent Systems and Computing, volume 1103 AISC, Springer, 2020, pp. 48–56, doi:10.1007/978-3-030-36664-3_6.
[23] E.A. Audenaert, C. Pattyn, G. Steenackers, J. De Roeck, D. Vandermeulen, P. Claes, Statistical shape modeling of skeletal anatomy for sex discrimination: their training size, sexual dimorphism, and asymmetry, Front Bioeng Biotechnol 7 (2019), doi:10.3389/fbioe.2019.00302.
[24] K. Imaizumi, K. Taniguchi, Y. Ogawa, K. Matsuzaki, H. Maekawa, T. Nagata, M. Mochimaru, M. Kouchi, Three-dimensional shape variation and sexual dimorphism of the face, nose, and mouth of japanese individuals, Forensic Sci. Int. 302 (2019), doi:10.1016/j.forsciint.2019.109878.
[25] P. Claes, A robust statistical surface registration framework using implicit function representations: Application in craniofacial reconstruction, K.U. Leuven, Belgium, 2007 Ph.D. thesis.
[26] D. Farnell, S. Richmond, J. Galloway, A. Zhurov, P. Pirttiniemi, T. Heikkinen, V. Harila, H. Matthews, P. Claes, An exploration of adolescent facial shape changes with age via multilevel partial least squares regression, Comput Methods Programs Biomed 200 (2021) 105935, doi:10.1016/j.cmpb.2021.105935.
[27] S. Shahidi, E. Bahrampour, E. Soltanimehr, A. Zamani, M. Oshagh, M. Moattari, A. Mehdizadeh, The accuracy of a designed software for automated localization of craniofacial landmarks on CBCT images, BMC Med Imaging 14 (1) (2014) 32, doi:10.1186/1471-2342-14-32.
[28] M. Codari, M. Caffini, G.M. Tartaglia, C. Sforza, G. Baselli, Computer-aided cephalometric landmark annotation for CBCT data, Int J Comput Assist Radiol Surg 12 (1) (2017) 113–121, doi:10.1007/s11548-016-1453-9.
[29] J. Montúfar, M. Romero, R.J. Scougall-Vilchis, Hybrid approach for automatic cephalometric landmark annotation on cone-beam computed tomography volumes, American Journal of Orthodontics and Dentofacial Orthopedics 154 (1) (2018) 140–150, doi:10.1016/j.ajodo.2017.08.028.
[30] B. Chakravarthy Neelapu, O.P. Kharbanda, V. Sardana, A. Gupta, S. Vasamsetti, R. Balachandran, H.K. Sardana, Automatic localization of three-dimensional cephalometric landmarks on CBCT images by extracting symmetry features of the skull, Dentomaxillofacial Radiology 47 (2018), doi:10.1259/dmfr.20170054.
[31] A.F. Ridel, F. Demeter, M. Galland, E.N. L'abbé, D. Vandermeulen, A.C. Oettlé, Automatic landmarking as a convenient prerequisite for geometric morphometrics. validation on cone beam computed tomography (CBCT)- based shape analysis of the nasal complex, Forensic Sci. Int. 306 (2020), doi:10.1016/j.forsciint.2019.110095.
[32] H.W. Hwang, J.H. Park, J.H. Moon, Y. Yu, H. Kim, S.B. Her, G. Srinivasan, M.N.A. Aljanabi, R.E. Donatelli, S.J. Lee, Automated identification of cephalometric landmarks: part 2-Might it be better than human? Angle Orthodontist 90 (1) (2020) 69–76, doi:10.2319/022019-129.1.
[33] H.S. Yun, T.J. Jang, S.M. Lee, S.H. Lee, J.K. Seo, Learning-based local-to-global landmark annotation for automatic 3D cephalometry, Phys Med Biol 65 (8) (2020) 85018, doi:10.1088/1361-6560/ab7a71.
[34] S. Nishimoto, Y. Sotsuka, K. Kawai, H. Ishise, M. Kakibuchi, Personal computer-based cephalometric landmark detection with deep learning, using cephalograms on the internet, Journal of Craniofacial Surgery 30 (1) (2019) 91–95, doi:10.1097/SCS.0000000000004901.
[35] S.H. Kang, K. Jeon, H.J. Kim, J.K. Seo, S.H. Lee, Automatic three-dimensional cephalometric annotation system using three-dimensional convolutional neural networks: a developmental trial, Computer Methods in Biomechanics and Biomedical Engineering: Imaging and Visualization 8 (2) (2020) 210–218, doi:10.1080/21681163.2019.1674696.
[36] G. Vitkus, Wars of lithuania: a systematic quantitative analysis of Lithuania's wars in the nineteenth and twentieth centuries, Eugrimas, Vilnius, 2014.
[37] J. Caple, C.N. Stephan, A standardized nomenclature for craniofacial and facial anthropometry, Int. J. Legal Med. 130 (3) (2015) 863–879, doi:10.1007/s00414-015-1292-1.
[38] W.W. Howells, Cranial variation in man: A Study by multivariate analysis of patterns of difference among recent human populations, Papers of the Peabody Museum of Archaeology and Ethnology, Harvard University 67 (1973) 1–259.
[39] O. Ibáñez, R. Vicente, D. Navega, C. Campomanes-Álvarez, C. Cattaneo, R. Jankauskas, M.I. Huete, F. Navarro, R. Hardiman, E. Ruiz, K. Imaizumi, F. Cavalli, E. Veselovskaya, D. Humpire, J. Cardoso, F. Collini, D. Mazzarelli, D. Gibelli, S. Damas, MEPROCS Framework for craniofacial superimposition: validation study, Leg Med 23 (2016) 99–108, doi:10.1016/j.legalmed.2016.10.007.
[40] J.G. Garson, The frankfort craniometric agreement, with critical remarks thereon., The Journal of the Anthropological Institute of Great Britain and Ireland 14 (1885) 64, doi:10.2307/2841484.
[41] J.D. White, A. Ortega-Castrillón, H. Matthews, A.A. Zaidi, O. Ekrami, J. Snyders, Y. Fan, T. Penington, S. Van Dongen, M.D. Shriver, P. Claes, Meshmonk: open-source large-scale intensive 3D phenotyping, Sci Rep 9 (1) (2019), doi:10.1038/s41598-019-42533-y.
[42] J. Snyders, P. Claes, D. Vandermeulen, P. Suetens, Development and Comparison of Non-Rigid Surface Registration Algorithms and Extensions, Technical Report, 2014. Technical report KUL/ESAT/PSI/1401 KU Leuven, ESAT, Leuven, Belgium
[43] A. Ecins, C. Fermuller, Y. Aloimonos, Seeing behind the Scene: Using Symmetry to Reason about Objects in Cluttered Environments, in: IEEE International Conference on Intelligent Robots and Systems, Institute of Electrical and Electronics Engineers Inc., 2018, pp. 7193–7200, doi:10.1109/IROS.2018.8593822.
[44] G. Bradski, The opencv library, Dr. Dobb's Journal of Software Tools (2000). https://opencv.org/
[45] J.L. Bentley, Multidimensional binary search trees used for associative searching, Commun ACM 18 (9) (1975) 509–517, doi:10.1145/361002.361007.
[46] O.J. Dunn, Multiple comparisons using rank sums, Technometrics 6 (3) (1964) 241–252, doi:10.1080/00401706.1964.10490181.
[47] R Core Team, R: A Language and environment for statistical computing, R Foundation for Statistical Computing (2020). https://www.r-project.org/
[48] A.H. Richard, C.L. Parks, K.L. Monson, Accuracy of standard craniometric measurements using multiple data formats, Forensic Sci. Int. 242 (2014) 177–185, doi:10.1016/j.forsciint.2014.06.015.
[49] A.C. Smith, A. Boaks, How "standardized" is standardized? a validation of postcranial landmark locations, J. Forensic Sci. 59 (6) (2014) 1457–1465, doi:10.1111/1556-4029.12576.
[50] N. Von Cramon-Taubadel, B.C. Frazier, M.M. Lahr, The problem of assessing landmark error in geometric morphometrics: theory, methods, and modifications, Am. J. Phys. Anthropol. 134 (1) (2007) 24–35, doi:10.1002/ajpa.20616.